Наносистеми, наноматеріали, нанотехнології
Nanosistemi, Nanomateriali, Nanotehnologii
2020, т. 18, № 3, сс. 529–539

PACS numbers: 61.46.Np, 68.37.Hk, 73.63.Fg, 82.45.Fk, 82.45.Yz, 82.47.Rs, 82.80.Fk

Self-Organized Anatase-Nanotubes' Array

A. I. Schurenko[1], V. I. Styopkin[1], D. O. Grynko[2], and A. M. Dobrovolskiy[1]

[1]*Institute of Physics, N.A.S. of Ukraine,*
46, Nauky Ave.,
UA-03028 Kyiv, Ukraine
[2]*V. Ye. Lashkaryov Institute of Semiconductor Physics, N.A.S. of Ukraine,*
45, Nauky Ave.,
UA-03028 Kyiv, Ukraine

The possibility of creating highly-ordered arrays of anatase nanotubes by means of anodizing and subsequent annealing under normal conditions is demonstrated. Annealing eliminates residues of organic impurities in the bulk of the structure after anodizing and subsequent purification too. The used electrolyte allows growing nanotubes with controlled geometric parameters within their internal diameter from 10 to 100 nm for exposure times from 10 to 40 min, and with lengths from 5 to 30 μm for times from 20 min to 9 hours. The possibility of using such structures as an electrode of electrochemical sensor systems of the DNA is shown.

Продемонстровано можливість створення високовпорядкованих масивів нанотрубок анатазу шляхом анодування та наступного відпалу в нормальних умовах. Відпал уможливлює також позбутися залишків органічних домішок в об'ємі структури після анодування та наступного очищення. Застосований розчин уможливлює вирощувати нанотрубки з керованими геометричними параметрами в межах їхнього внутрішнього діяметра від 10 до 100 нм для часів експозиції від 10 до 40 хв. і довжини від 5 до 30 мкм за час від 20 хв. до 9 годин. Показано можливість використання таких структур у якості електроди ДНК-сенсорних електрохемічних систем.

Key words: nanotubes array, anatase, anodization, electrochemical sensor system, DNA.

Ключові слова: масиви нанотрубок, анатаз, анодування, електрохемічні сенсорні системи, ДНК.

(Received 7 April, 2020)

1. INTRODUCTION

Titanium dioxide itself can be considered a material of the last century. This material finds its application in an increasing number of areas and aspects of the human being. It is already used in the construction industry and in medicine, both in the form of modifying coatings and individual nanoparticles. The structured layers of titanium dioxide are of particular interest. They attract attention due to their interesting physical and electrochemical properties, high biocompatibility and the ability to create self-assembled structures over a large surface area [1, 2]. Such structures can be used in photocatalysis systems [2–5], hydrogen generation [6, 7], solar panels [8–10], sensor systems [5, 11], when creating self-cleaning surfaces and biocompatible materials, including the targeted delivery of drugs to the prosthetic site [12, 13]. It should be noted separately that the situation of application of such layers for increasing the contact surface area in the electrode–liquid systems used in electroanalysis [14].

Due to such a wide range of applications of ordered nanotubes arrays, the interest in their synthesis has not subsided for several decades. The method of their creation by the anodization of a titanium electrode in solutions of electrolytes containing fluorine is widely known, relatively simple and easily scalable [15]. It is also important fact that this method allows to control within certain limits the parameters of the obtained structures—the length of the tubes and their diameters. From a scientific point of view, there is a partial understanding of the process of creating a separate nanotube during titanium anodization, but questions remain about the ordered growth of the array as a whole [16].

In electrochemical devices working with control solutions, the surface area of the electrode plays a significant role in determining the sensitivity of the method as a whole. Therefore, different methods of surface structuring at the macro and micro levels are important for improving their characteristics.

The purpose of our work is to create ordered arrays of anatase nanotubes with controlled geometry and to verify the possibility of their use in electrochemical systems for diagnostics of certain types of DNA molecules.

2. EXPERIMENTAL

The anodization of titanium foil was done in the simplest reactor with two electrodes. The pH level was not monitored. As a working electrode, we used a titanium foil with a thickness of 110 μm with a titanium content of 99.93%. The sample size was 10×20 mm. The anodizing occurred in a Teflon reservoir with dimensions 25×40×35 mm. The so-

lution containing ethylene glycol, NH_4F, and distilled H_2O was used as the electrolyte. A constant voltage was used in the range of 30 to 80 V, and the anodizing time was varied from 10 min to 9 hours. The progress of the nanotube growth process was monitored by a well-known current–time characteristic (Fig. 1). One can see from the graph that the formation of the initial oxidation layer occurs in less than 10 minutes, and then, we can influence the geometric parameters of the obtained pores and nanotubes by changing the anodizing time from 10 minutes to the required time.

The phase state of the created layer and its purity was monitored using Raman spectroscopy and the morphology was evaluated by scanning electron microscopy (SEM). Layer of nanotubes created by the anodizing can be separated from the foil for obtaining either a membrane of TiO_2 or powders of fragments of an array of nanotubes, after mechanical milling of the obtained membranes. In Figure 2, one can see an

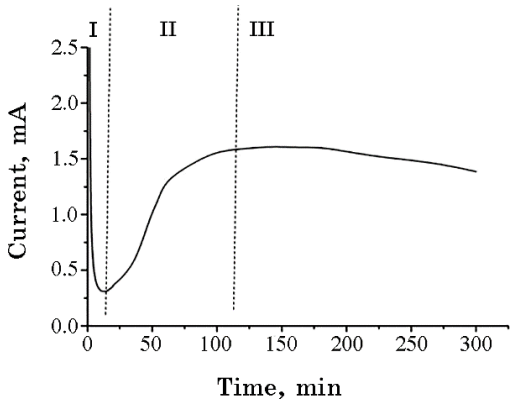

Fig. 1. Typical current–time characteristic of a titanium foil anodizing process. I—stage of oxidation layer formation on a titanium; II—stage of forming the pores and the nanotubes; III—stage of the process coming to stationary state.

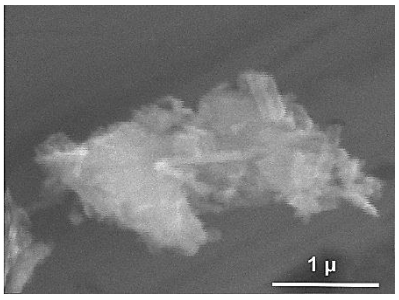

Fig. 2. SEM image of the powder of TiO_2 nanotubes' fragments.

example of the obtained powder.

3. RESULTS

The selected electrolyte has a reduced activity for dissolving of the TiO_2 layer as compared to previously used aqueous solutions with fluorine content. The latter allows controlling more precisely the process of formation of arrays of nanotubes due to their slower formation. In the selected electrolyte, the inner diameter of the tube exhibits a virtually linear dependence of the exposure time in the range of 10 to 100 nm for exposure times of 10 to 40 minutes. Also close to linear, there is the dependence of the length of the grown nanotubes on the anodizing time. The length of the nanotubes synthesized over a period of 20 min

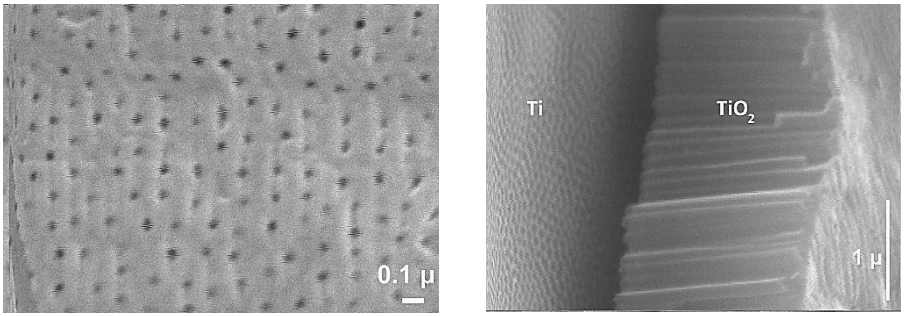

a *b*

Fig. 3. SEM images of TiO_2 nanotube arrays obtained for normal orientation of surface to electron beam (*a*) and for tilt at 60° from normal position; anodizing conditions: 60 V, 30 minutes.

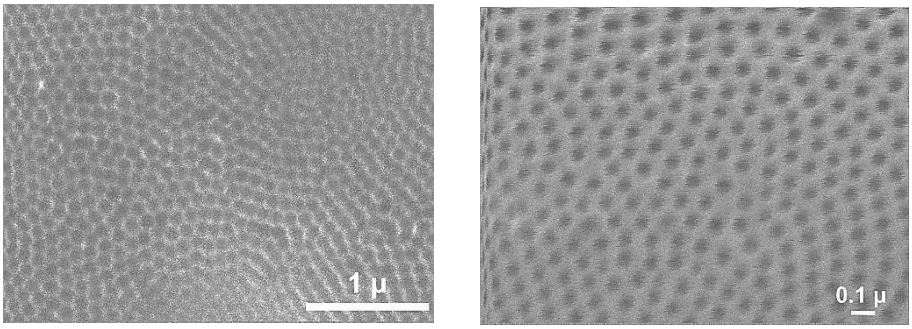

a *b*

Fig. 4. The typical SEM image of the titanium surface after removal of the first anodizing layer (*a*), and the image of the TiO_2 array surface obtained by repeated anodizing (*b*).

to 9 hours varied from 5 to 30 μm.

Examples of SEM images of the resulted arrays are shown in Fig. 3. The images show that the tubes grow with very high quality and pass through the entire thickness of the layer for all experimental conditions. However, the packing density per unit of the layer surface remains virtually unchanged for all conditions. We can state that only the thickness of the tube wall changes. Although the first anodization demonstrates good self-organization of the array, local disturbances of the order are also noticeable.

At the same time, in Fig. 3, *b*, one can see the surface of titanium under the created layer of nanotubes. It is noticeable that the cavities on the surface of the titanium are very well arranged and are as tight as possible to each other, despite the sparse location of the cavities on the surface of the film. This gives reason to try obtaining highly ordered arrays by double anodizing.

In Figure 4 the SEM images of the array of Ti cavities and TiO_2 nanotubes obtained by double anodizing are given. For that purpose, the initially grown first layer of nanotubes is removed from the base and a new layer is grown on the resulted nanorelief of the Ti surface under similar conditions.

One can see from the obtained results that repeated anodizing allows creating highly ordered arrays of nanotubes. However, the resulted arrays consist mainly of amorphous titanium dioxide. This is evidenced by their Raman spectra shown in Fig. 5.

The spectrum of the sample before its annealing shows only characteristic bands of amorphous Titania and does not contain lines of crystallized titanium dioxide. There are also peaks in the spectrum that we

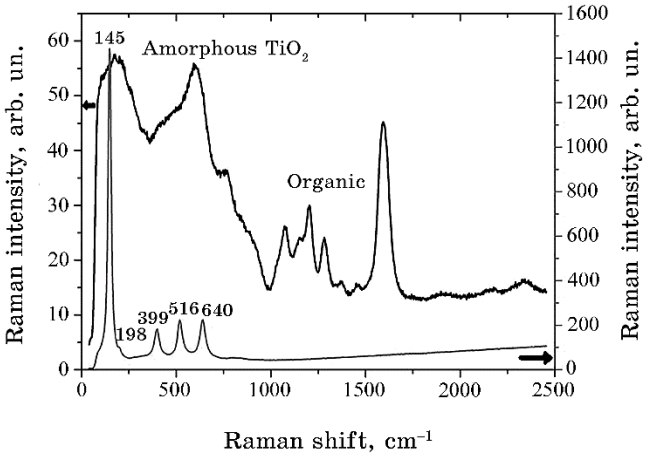

Fig. 5. Raman spectra of the nanotubes arrays before (upper curve) and after (lower curve) the annealing.

associate with the presence of organic contaminants in the sample remaining after anodizing and the subsequent washing of the samples. After annealing in air at a temperature of 430°C for two hours, the spectrum changes dramatically. The peaks on the right side disappear and the amorphous dioxide band is restructured into anatase-specific spectrum. (The spectrum is obtained by means of a DFS-52 spectrometer.)

The titanium foil structured by the nanotubes (TiNAN) was used as the electrode of the electrochemical sensor system. The obtained results were compared with those of conventional thermally oxidized ti-

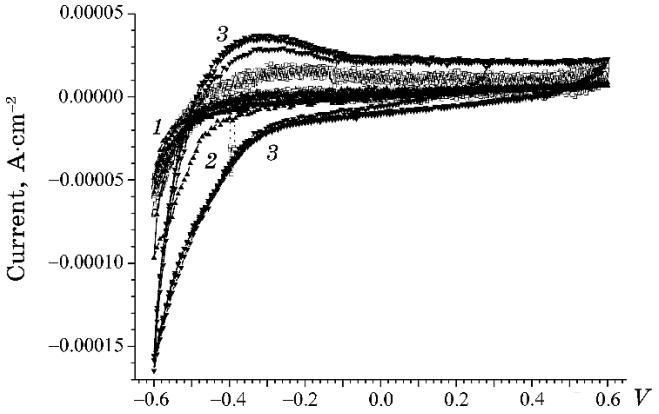

Fig. 6. Current–voltage characteristics of TiNAN electrode (*3*) and TiO_X electrode (*2*) in comparison to stainless NiCr steel electrode (*1*) in the 250 mM potassium dihydrophosphate electrolyte.

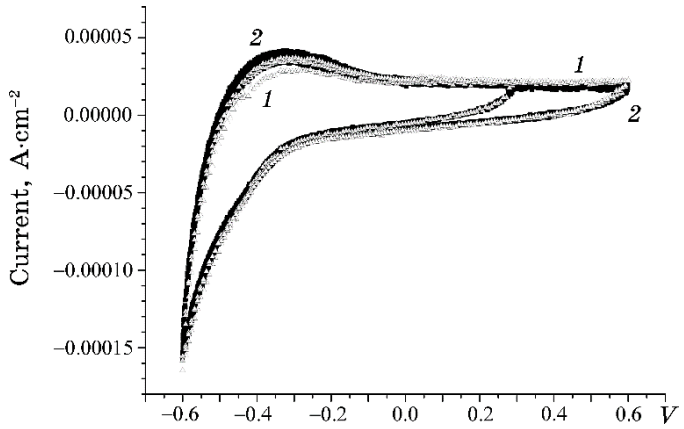

Fig. 7. Current–voltage characteristics of TiNAN electrode before (*1*) and after (*2*) immobilization with mod-Ph thiolated oligonucleotide in the 1 mkM mod-Ph and 250 mM potassium dihydrophosphate electrolyte.

tanium (TiO_X) and stainless NiCr steel alloy. Current–voltage curves of titanium oxide-based electrodes in the 250 mM potassium dihydrophosphate electrolyte (presented on Fig. 6) are similar to characteristic of stainless steel electrode. The main distinctive feature of current-voltage curves is electrodes capacity value, which can be calculated proportionally to the area of current–voltage loop. Electrodes capacity value is arranged with the decreasing series: TiNAN > TiO_X > NiCr.

Immobilization with mod-Ph thiolated oligonucleotide [17, 18] was investigated. The ability to qualitatively distinguish the structure of hybridized molecular layers was demonstrated with P1 oligonucleotide, which is complementary to mod-Ph. As a medium for immobilization of thiolated oligonucleotides on the surface of the semiconductor electrodes solution 250 mm KH_2PO_4 (pH 4) was used. And for hybridization of P1 oligonucleotide buffer, solution 0.5×SSC (pH 7.4) was used.

Titanium oxide is a well-known *n*-type semiconductor with a high density of negatively charged surface states. In contrast to models [17, 18] related to a gold electrode, we expected to observe the binding of the thiol group of mod-Ph artificial DNA with negatively charged centres on the surface of titanium oxides. Some differences in the current–voltage characteristics (Fig. 7) explained by molecular shell formation and cannot be caused by bulk conductivity variation of electrolyte due to small variation of its concentration. Current–voltage characteristics and complex impedance after the hybridization mod-Ph with P1 oligonucleotides of TiNAN and TiO_X-based electrodes were demonstrated in Figs. 8, 9.

Capacity of electrode can be calculated as an effective parallel capacity of impedance measurements data and generally can be related to the structure of electrode–electrolyte interface and Helmholtz layer. Capacity of titanium and NiCr electrodes in relation to frequency is represented in Fig. 10. The capacity of the NiCr electrode does not varies significantly in the frequency range 1 Hz–100 kHz. Since its capacity does not change after processing in oligonucleotides solutions, we can conclude that the molecular shell was not formed.

Capacity of TiO_X electrode is approximately the same as capacity of NiCr electrode at lower frequencies. Thermal oxide TiO_2 thickness was estimated from capacity value of 4 nm. Relation of decreasing of TiO_X electrode capacity to frequency can be explained by reduction of polarizability of the Helmholtz layer when oxide TiO_2 thickness is the same as arranged ion layer thickness. Capacity of TiNAN electrode is few times higher than TiO_X capacity because of large value of its nanostructured surface. But the value of capacities difference of TiO_X and TiNAN is much smaller than anticipated, considering nanostructured surface values (Figs. 3, 4).

Formation of oligonucleotide shell on the surface of TiNAN elec-

trode gives rise of capacity in contrary to TiO_X, which may be explained by the time lag of proton extraction—enrichment in the nanotubes of TiNAN and molecular layer polarization reduction with frequency raise.

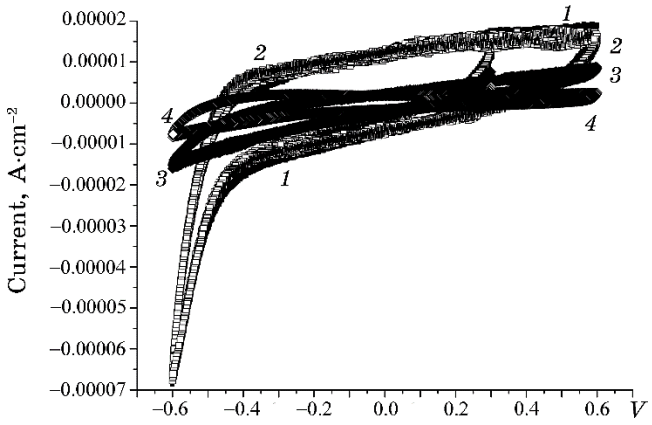

Fig. 8. Current–voltage characteristics of TiNAN electrode (*1*, *2*) and TiO_X one (*3*, *4*) before (*1*, *3*) and after (*2*, *4*) hybridization of mod-Ph and P1 oligonucleotides in the 10nM P1 0.5 SSC solution. Noticeable differences in the current–voltage characteristics (Fig. 8) and impedance curves (Fig. 9) of both titanium oxide-based electrodes before and after hybridization of mod-Ph and P1 oligonucleotides caused by formation of oligonucleotides molecular shells on the surface of electrodes and may be applied to sensor task.

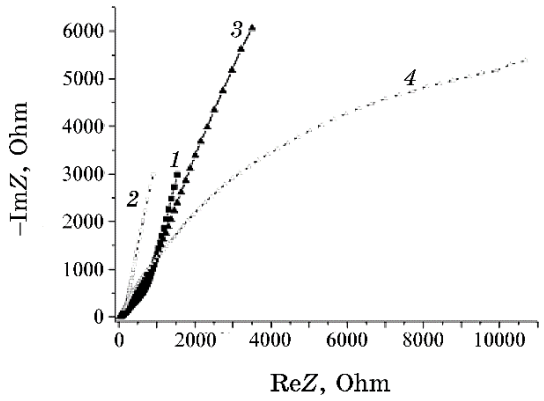

Fig. 9. Impedance *Z* of electrochemical system with TiNAN (*1*, *2*) and TiO_X (*3*, *4*) electrodes with oligonucleotides shell in the 0.5 SSC electrolyte at frequency range of 1 Hz–100 kHz: *1*, *3*—before hybridization, and *2*, *4*—after hybridization of mod-Ph and P1 in the 10nM P1 0.5 SSC solution. (Im*Z*—imaginary value of *Z*, and Re*Z*—real value.)

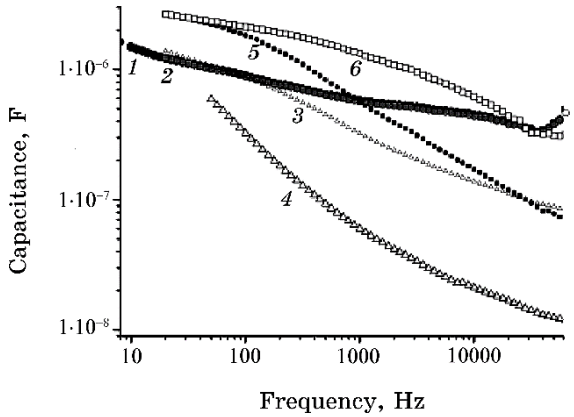

Fig. 10. Capacity of electrodes before (*1*, *3*, *5*) and after realization of the treatment for the immobilization of mod-Ph and hybridization mod-Ph with P1 in the 10 nM P1 and 0.5 SSC solution for electrodes: *1*, *2*—NiCr; *3*, *4*—TiO_X; *5*, *6*—TiNAN.

The results of mod-Ph-P1 hybridization studies using titanium oxide electrodes in Figs. 8–10 indicate that nanostructured titanium can be considered a promising high-performance electrochemical electrode sensor material.

The significance of above presented self-organized anatase nanotubes array as well as self-organized semi-conductive nanocrystals array [19–22] is a shared nanosize system with size effect response onto a molecular level structure variations such as charge, mass, conductivity, capacitance, morphology, density near to the solid–molecular interface. Variations of molecular layer polarizability, charge, added mass, conductivity, capacitance, morphology, density are the mean mesoscopic manifestation of selective recognizing of biologically important markers due to DNA hybridization or similar specific surface reactions. These mesoscopic variations of the state of monomolecular layer effecting on the proximal thin surface layer of semiconductor with well-predicted and strong impacts on its conductivity, energy states, optical or mechanical properties. The thickness of this surface layer is 30–100 nm.

Fabrication of semiconductor in the form of well-branched morphology with typical semiconductor layer thickness 50–200 nm producing sensitive system, which is capable to generate maximum response signal. In our previous work, brush-type nanocrystals topology [21, 22, 23] of CdS nanosize self-organized nanocrystals on the surface of pyrolytic carbon micro-wire at the first–second hierarchical levels and thiolated oligonucleotide mod-Ph and oligonucleotide P1 at the third level were used. The synthesized semi-conductive nanostructured electrodes with the functionalized shell of mod-Ph may allow to detect

qualitatively and quantitatively the selective sorption of synthetic DNAs P1 at a concentration of 10 nM in an actual biologically solutions by conductivity and impedancemetry methods.

The fabrication of nanodevices by controlling the growth of nanocrystals or the formation of nanotubes in bottom-up approach in combination with the traditional CMOS technology is a rather effective and inexpensive technology for the production of universal matrix sensor devices in which the first and second hierarchical levels of the sensor are implemented. Selective recognition of biologically important markers can be organized at the third hierarchical level by formation of molecular biological shells of DNA markers on the surface of the sensitive elements of this matrix-type sensor device.

4. CONCLUSIONS

The obtained results demonstrate the possibility of synthesis of highly ordered arrays of anatase nanotubes by single and double anodization with their subsequent annealing in air under normal conditions. The resulted arrays demonstrate high purity from residual contamination and good homogeneity of the polymorphic state. Such arrays can be applied for medical purposes and sensor electrochemical systems.

The used method allows practically linear control of geometrical parameters of the nanotubes within their internal diameter from 10 to 100 nm for exposure times from 10 to 40 min and length from 5 to 30 μm for the time from 20 min to 9 hours.

The results of mod-Ph-P1 hybridization studies using impedance measurements with titanium oxide electrodes indicate that nanostructured titanium can be considered a promising high-performance electrochemical electrode sensor material. It's shown the possibility of using the obtained TiO_X structures in electrochemical systems with specific DNAs at the boundary of the electrodes with the electrolyte. The formation of molecular shells on the surface of anatase nanotubes and their selective binding to synthetic DNA P1 by conductivity and impedancemetry methods in the frequency range 100 kHz–1 Hz was investigated. The qualitative difference between the structures of charged and polarized organic molecular layers at the boundary of self-organized anatase nanotubes with SSC electrolytes was demonstrated.

REFERENCES

1. X. Wang, Z. Li, J. Shi, and Y. Yu, *Chemical Reviews*, **114**, No. 19: 9346 (2014); https://doi.org/10.1021/cr400633s.
2. Y. Ye, Y. Feng, H. Bruning, D. Yntema, and H. H. M. Rijnaarts, *Applied Catalysis B: Environmental*, **220**: 171 (2018);

http://dx.doi.org/10.1016/j.apcatb.2017.08.040.
3. N. Liu, I. Paramasivam, M. Yang, and P. Schmuki, *J. Solid State Electr.*, **16**: 3499 (2012).
4. H. Song, K. Cheng, and H. Guo, *Catalysis Communication*, **97**: 23 (2017).
5. Q. Zhou, Z. Fang, J. Li, and M. Wang, *Microporous and Mesoporous Materials*, **202**: 22 (2015).
6. S. Hejazi, N. T. Nguyen, A. Mazare, and P. Schmuki, *Catal. Today*, **281**, Part 1: 189 (2017).
7. M. Ge, Q. Li, C. Cao, *Adv. Sci.*, **4**: 1600152 (2017); https://doi.org/10.1002/advs.201600152.
8. F. Mohammadpour, M. Moradi, and G. Cha, *Chemelectrochem*, **2**: 204 (2015).
9. X. Gao, J. Li, J. Baker, and Y. Hou, *Chem. Commun.*, **50**: 6368 (2014).
10. A. Pourandarjani and F. Nasirpouri, *Thin Solid Films*, **640**: 1 (2017).
11. M. Terracciano, V. Galstyan, I. Rea, and M. Casalino, *Appl. Surf. Sci.*, **419**: 235 (2017).
12. M. Kulkarni, A. Mazare, and E. Gongadze, **26**: 062002 (2015).
13. A. Pawlik, M. Jarosz, K. Syrek, and G. D. Sulka, *Colloid and Surface B: Biointerfaces*, **152**: 95 (2017).
14. A. Walcarius, *Anal Bioanal Chem.*, **396**: 261 (2010).
15. A. I. Schurenko, V. I. Stiopkin, D. A. Galaktionov, O. V. Danko, P. I. Lytvin, and D. O. Grynko, *Nanophysics, Nanophotonics, Surface Studies, and Applications. Vol. **183**. Springer Proceedings in Physics* (Eds. O. Fesenko and L. Yatsenko), p. 179 (2016); doi 10.1007/978-3-319-30737-4_15.pp.
16. Yu Fu and Anchun Mo, *Nanoscale Research Letters*, **13**: 187 (2018); doi 10.1186/s11671-018-2597-z.
17. M. Matsishin, A. Rachkov, A. Errachid, S. Dzyadevych, and A. P. Soldatkin, *Sensors and Actuators B-Chemical*, **222**: 1152 (2016).
18. M. J. Matsishin, Iu. V. Ushenin, A. E. Rachkov, and A. P. Solatkin, *Nanoscale Research Letters*, **11**: 19 (2016); doi 10.1186/s11671-016-1226-y.
19. A. B. Bogoslovska, O. M. Khalimovskyy, and D. O. Grynko, *Semiconductor Physics, Quantum Electronics and Optoelectronics*, **22**: 479 (2019).
20. A. Bogoslovska, D. Grynko, E. Bortchagovsky, and O. Gudymenko, *Semiconductor Physics, Quantum Electronics and Optoelectronics*, **22**: 231 (2019).
21. P. S. Smertenko, D. A. Grynko, N. M. Osipyonok, O. P. Dimitriev, and A. A. Pud, *Phys. Stat. Solidi A*, **210**, No. 9: 1851 (2013); doi: 10.1002/pssa.201228805.
22. D. A. Grynko, O. M. Fedoryak, P. S. Smertenko, O. P. Dimitriev, N. A. Ogurtsov, and A. A. Pud, *Nanoscale Research Letters*, **11**, No. 1: 265 (2016); doi: 10.1186/s11671-016-1469-7.
23. D. Grynko, A. Rachkov, and A. Soldatkin, *Abstracts of NANSYS-2019 Conf. (3–5 December 2019, Kyiv, Ukraine)* (Kyiv: N.A.S.U.: 2019), p. 200.